Refractive-index matching between liquid crystals and photopolymers

Jun Li
Greg Baird
Yi-Hsin Lin
Hongwen Ren
Shin-Tson Wu

Abstract — Refractive indices of two photocurable polymers, NOA65 and NOA81 (Norland Optical Adhesive), and two series of Merck liquid crystals, E-series (E44, E48, and E7) and BL-series (BL038, BL003 and BL006), and two UCF high-birefringence liquid-crystal mixtures were measured using an Abbe refractometer in the visible spectral region and 15–55°C temperature range. Some liquid crystals have excellent index matching with NOA65 in the red, while some fit better in the blue spectral region. To validate this index-matching property found in the material level, we prepared some polymer-dispersed liquid-crystal devices. Good correlations between material and device performances are obtained.

Keywords — *Liquid crystals, Norland polymers, refractive index, polymer-dispersed liquid crystals.*

1 Introduction

Polymer-dispersed liquid crystal (PDLC) and polymer-stabilized liquid crystal (PSLC) are useful for displays,[1–4] tunable wavelength filters,[5–7] tunable liquid-crystal lenses,[8,9] and polarization-independent phase modulators.[10] In a PDLC, the refractive-index difference between the LC droplets and polymer matrix plays an important role in determining the voltage-off and voltage-on state transmittance. In a normal-mode PDLC, the droplet size is controlled at ~1 μm, which is comparable with the visible-light wavelength. In the voltage-off state, the droplets are randomly oriented. The index mismatch between the LC (whose average refractive index is given by $\langle n \rangle = (n_e + 2n_o)/3$) and polymer matrix ($n_p$) affects the light-scattering capability. For a given droplet size, the larger the index mismatch, the higher the light scattering. Conversely, in the voltage-on state the LC directors inside the droplets are reoriented along the electric-field direction so that the refractive index becomes n_o; the ordinary refractive index. If $n_o \sim n_p$, then the PDLC becomes isotropic and will have an excellent transmittance. Therefore, the preferred LC material for PDLC is not only high birefringence ($\Delta n = n_e - n_o$) but also good index match between n_o and n_p. In a PSLC system, polymer networks help to improve response time.[11] A good index match would reduce light scattering.

In this paper, we compare the refractive index of cured polymers with liquid crystals at different wavelengths and temperatures. In Section 2, the fabrication method of the thin cured polymer films is briefly described. The refractive index of the cured polymer films (NOA65 and NOA81) and six nematic liquid crystals (BL038, BL006, BL003, E48, E44, and E7) were measured using a multi-wavelength Abbe refractometer. In Section 3, we compare the refractive index between NOA 65 and these six commercial liquid crystals, and NOA81 with two UCF high birefringence mixtures: UCF-1 and UCF-2. In Section 4, we fabricate some PDLC cells using the four selected index-matched LC mixtures in the NOA65 polymer system and characterize their electro-optic properties at λ = 633 nm. In Section 5, we obtain good correlation between material and device performances.

2 Measurements of refractive indices

NOA65 (Norland Optical Adhesive) is a commonly used photocurable polymer because its refractive index ($n_p \sim 1.52$) is close to the n_o of many commercial LC mixtures. On the other hand, NOA81 has a higher refractive index ($n_p \sim 1.56$), which is close to the n_o of our UCF high-birefringence LC mixtures. In this study, we compare the refractive indices of NOA65 with six Merck LC mixtures, and NOA81 with two UCF high birefringence LC mixtures using a multiwavelength Abbe refractometer (Atago DR-M4). Before UV curing, NOA65 and NOA81 are clear and colorless liquids. The measurement of the monomers is fairly simple. However, in a practical device, such as a PDLC, all the monomers are cured to form a polymer matrix. Therefore, it is more meaningful to measure the refractive index of the cured polymers than the monomers.

In order to fabricate a polymer film, we infiltrated the monomers into an empty cell with a 1-mm gap using capillary flow. The cells were placed on a hot plate with a constant temperature (T ~ 50°C). Then, we illuminated the cell with a uniform UV light (I = 14 mW/cm^2, λ ~ 365 nm) for 40 minutes because of the large cell gap. We then peeled off the glass substrates and removed the thick polymer film under a high temperature (T ~ 120°C). The film was kept in a stove with a constant temperature of 50°C for 12 hours to age completely. The cured polymer film of NOA65 is quite flexible, while the cured NOA81 is a little rigid. In order to get an accurate measurement, we cut the films into rectangular parallelepipeds of the following dimensions: 15 mm long, 9 mm wide, and 1 mm thick. The bottom surface of the samples was polished so that it made contact with the main prism surface of the Abbe refractometer completely. First,

The authors are with the College of Optics and Photonics, University of Central Florida, Orlando, FL 32816, U.S.A.; telephone 407/823-4763, fax 407/823-6880, e-mail: swu@mail.ucf.edu.

© Copyright 2005 Society for Information Display 1071-0922/05/1312-1017$1.00

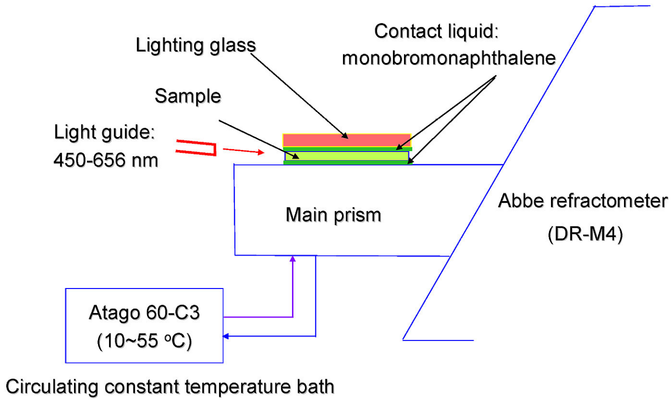

FIGURE 1 — The experimental setup for measuring the refractive index of cured polymer films: NOA65 and NOA81.

we put a small drop of contact liquid (monobromonaphthalene) on the main prism, then put the sample on and ensured the contact liquid spread evenly between the sample and the main prism. It is important to get rid of any dust and bubbles between the solid sample and the main prism. A lighting glass was used to compensate for the weak light because the samples are thin. Similarly, we spread a small amount of the contact liquid on the top surface of the sample and put the lighting glass on top of the contact liquid. The thin contact liquid should spread evenly between the sample and the lighting glass. Now the contact liquid is sandwiched as films between the main prism and the sample and between the sample and the lighting glass. The incident light entered the sample slightly aslant from the upside.

Figure 1 shows the experimental setup for measuring the cured polymer films. By moving the lighting glass to the front and rear, pressing the lighting glass to the sample by fingers, and adjusting the height and angle of the light guide, we found a clear and correct boundary line. This is the sign for the accurate measurements using the Abbe refractometer. We measured the refractive indices of LCs and polymers at six wavelengths: 450, 486, 546, 589, 633, and 656 nm. By connecting a constant circulating temperature bath (Atago 60-C3) with the Abbe refractometer, we measured the temperature-dependent refractive index of the samples from 15 to 55°C at 5°C intervals.

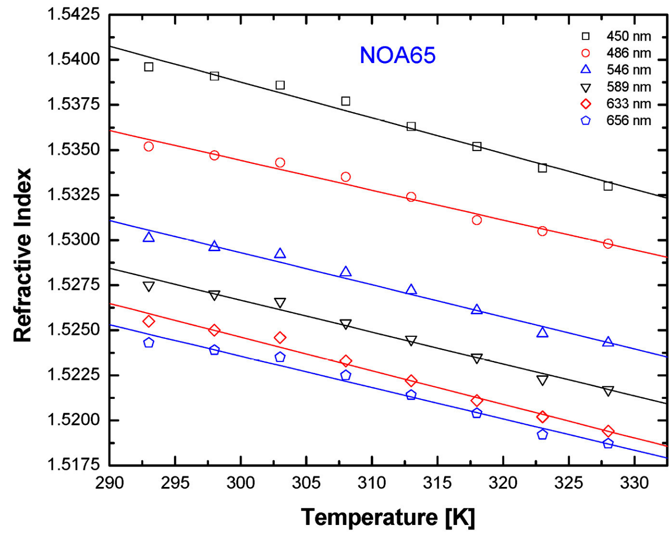

FIGURE 2 — Wavelength- and temperature-dependent refractive index of cured NOA65. The squares, circles, upward triangles, downward triangles, diamonds, and pentagons represent the measured refractive index of NOA65 at λ = 450, 486, 546, 589, 633, and 656 nm, respectively. Solid lines are fittings using Eq. (1) and the fitting parameters are listed in Table 1.

Figure 2 shows the wavelength- and temperature-dependent refractive index of the cured NOA65 polymer. The squares, circles, upward triangles, downward triangles, diamonds, and pentagons represent the measured refractive index of NOA65 at λ = 450, 486, 546, 589, 633, and 656 nm, respectively. In Fig. 2, we find the refractive index of NOA65 decreases linearly as temperature increases at a given wavelength:

$$n(T) = A - BT, \tag{1}$$

where the A and B coefficients in Eq. (1) are constant at a given wavelength. The fitting values of A and B are listed in Table 2. This linear decrease with increasing temperature might be related to the isotropic nature of NOA65. As the temperature increases, the density of most of the isotropic

TABLE 1 — The measured refractive index of cured NOA65 film at λ = 450, 486, 546, 589, 633, and 656 nm at different temperatures.

T (°C) \ n	λ (nm) 450	486	546	589	633	656
20	1.5396	1.5352	1.5301	1.5275	1.5255	1.5243
25	1.5391	1.5347	1.5296	1.5270	1.5250	1.5239
30	1.5386	1.5343	1.5292	1.5266	1.5246	1.5235
35	1.5377	1.5335	1.5282	1.5254	1.5233	1.5225
40	1.5363	1.5324	1.5272	1.5245	1.5222	1.5214
45	1.5352	1.5311	1.5261	1.5235	1.5211	1.5204
50	1.5340	1.5305	1.5248	1.5223	1.5202	1.5192
55	1.5330	1.5298	1.5243	1.5217	1.5194	1.5187

TABLE 2 — The fitting parameters for the refractive index [Eq. (1)] of NOA65 and NOA81 at λ = 450, 486, 546, 589, 633, and 656 nm.

	NOA65		NOA81	
λ (nm)	A	B (K^{-1})	A	B (K^{-1})
450	1.5983	1.98×10^{-4}	1.6305	1.68×10^{-4}
486	1.5841	1.65×10^{-4}	1.6110	1.20×10^{-4}
546	1.5828	1.78×10^{-4}	1.5988	1.01×10^{-4}
589	1.5797	1.77×10^{-4}	1.5995	1.13×10^{-4}
633	1.5801	1.86×10^{-4}	1.6039	1.36×10^{-4}
656	1.5758	1.74×10^{-4}	1.5994	1.25×10^{-4}

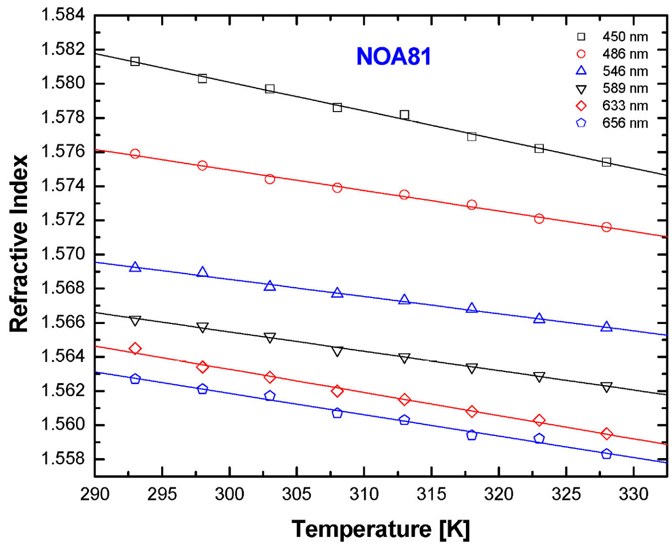

FIGURE 3 — Wavelength- and temperature-dependent refractive index of cured NOA81. The squares, circles, upward triangles, downward triangles, diamonds, and pentagons represent the measured refractive index of NOA81 at λ = 450, 486, 546, 589, 633, and 656 nm, respectively. Solid lines are fittings using Eq. (1) and the fitting parameters are listed in Table 3.

organics decreases which, in turn, causes the refractive index to decrease linearly.

Figure 3 shows a similar plot for NOA81. The squares, circles, upward triangles, downward triangles, diamonds, and pentagons represent the measured refractive index of NOA81 at λ = 450, 486, 546, 589, 633, and 656 nm, respectively. Similarly to NOA65, the refractive index of NOA81 decreases linearly as the temperature increases. The solid lines in Fig. 3 are fittings using Eq. (1) and the fitting parameters are listed in Table 2. We also measured the wavelength- and temperature-dependent refractive index of NOA65 and NOA81 in the monomer state. After UV curing, the refractive index of the cured polymers increases 1.7% and 2.2% for NOA65 and NOA81, respectively. This slight refractive-index increase originates from the increased density of the polymer after cross-linking.

For a normal-mode PDLC, the light scattering in the voltage-off state depends on the LC birefringence; the higher the birefringence, the higher the scattering efficiency. In the voltage-on state, the transmittance depends on the refractive index match between the LC (n_o) and the polymer matrix (n_p). If $n_o \sim n_p$, then the on-state will be highly transparent. After having measured the n_p of NOA65,

TABLE 3 — The measured refractive index of cured NOA81 film at λ = 450, 486, 546, 589, 633, and 656 nm at different temperatures.

T (°C) \ n	λ (nm) 450	486	546	589	633	656
20	1.5814	1.5759	1.5692	1.5662	1.5645	1.5627
25	1.5803	1.5752	1.5689	1.5658	1.5634	1.5621
30	1.5797	1.5744	1.5681	1.5652	1.5628	1.5617
35	1.5786	1.5739	1.5677	1.5644	1.562	1.5607
40	1.5782	1.5735	1.5673	1.564	1.5615	1.5603
45	1.5769	1.5729	1.5668	1.5634	1.5608	1.5594
50	1.5762	1.5721	1.5662	1.5629	1.5603	1.5586
55	1.5754	1.5716	1.5657	1.5623	1.5595	1.5583

we selected two commercial high birefringence LC series with their n_o close to n_p. The two LC series are BL-series (BL038, BL006, and BL003) and E-series (E48, E44, and E7). To measure the refractive indices, we aligned the LCs perpendicular to the main and secondary prism surfaces of the Abbe refractometer by coating these two surfaces with a surfactant comprising of 0.294 wt.% hexadecyletrimethyle-ammonium bromide (HMAB) in methanol solution. The measured extraordinary (n_e) and ordinary (n_o) refractive indices of E48, E44, E7, BL038, BL006, and BL003 are listed in Tables 5–10, respectively. From this data, we find that n_e always decreases as temperature increases, whereas n_o declines modestly first and then increases after the temperature passes the crossover temperature.[12] The average refractive index $\langle n \rangle$ [which is defined as $(n_e + 2n_o)/3$] also decreases linearly as temperature increases.[13]

The wavelength-dependent refractive index of the UV-cured polymers can be described by the extended Cauchy equation,[14–16]

$$n(\lambda) = A + \frac{B}{\lambda^2} + \frac{C}{\lambda^4}. \qquad (2)$$

Here, A, B, and C are Cauchy coefficients which are constant at a given temperature.

3 Refractive-index comparisons

NOA81 (n_p ~ 1.56) has a higher refractive index than NOA65 (n_p ~ 1.52). For a linearly conjugated LC, a high n_o often leads to a high Δn. Most of the commercially available

TABLE 4 — The fitting parameters for the refractive index [Eq. (2)] of NOA65 and NOA81 and the ordinary refractive index of E48, E44, E7, BL038, BL006, BL003, UCF-1, and UCF-2 at _ = 20°C.

Cauchy coefficients	NOA65	E48	E44	E7	BL038	BL006	BL003	NOA81	UCF-1	UCF-2
A	1.5130	1.5027	1.5018	1.4995	1.5042	1.5034	1.5056	1.5519	1.5439	1.5422
B (μm^2)	0.0045	0.0055	0.0089	0.0068	0.0065	0.0085	0.0057	0.0036	0.0038	0.0043
C (μm^2)	1.8×10^{-4}	5.6×10^{-4}	1.0×10^{-4}	4.1×10^{-4}	4.7×10^{-4}	1.9×10^{-4}	5.9×10^{-4}	4.9×10^{-4}	0.0019	0.0018

TABLE 5 — The measured refractive indices (n_e and n_o) of E48 at λ = 450, 486, 546, 589, 633, and 656 nm at different temperatures.

T	λ (nm) 450		486		546		589		633		656	
(°C)	n_e	n_o	n_e	n_o	n_e	n_o	n_e	n_o	n_e	n_o	n_e	n_o
15	1.8209	1.5399	1.7969	1.5366	1.7715	1.5282	1.7593	1.5239	1.7503	1.5204	1.7463	1.5195
20	1.8151	1.5391	1.7912	1.5360	1.7660	1.5274	1.7539	1.5233	1.7451	1.5197	1.7408	1.5186
25	1.8086	1.5384	1.7850	1.5353	1.7601	1.5268	1.7481	1.5225	1.7391	1.5188	1.7354	1.5175
30	1.8017	1.5403	1.7782	1.5342	1.7542	1.5261	1.7423	1.5217	1.7335	1.5180	1.7298	1.5165
35	1.7942	1.5403	1.7720	1.5345	1.7478	1.5255	1.7362	1.5214	1.7275	1.5176	1.7235	1.5161
40	1.7869	1.5406	1.7649	1.5337	1.7411	1.5252	1.7298	1.5206	1.7210	1.5172	1.7169	1.5158
45	1.7780	1.5395	1.7575	1.5336	1.7338	1.5250	1.7226	1.5206	1.7140	1.5168	1.7106	1.5156
50	1.7704	1.5399	1.7489	1.5339	1.7263	1.5250	1.7152	1.5205	1.7071	1.5167	1.7034	1.5151
55	1.7608	1.5392	1.7399	1.5343	1.7176	1.5252	1.7070	1.5207	1.6989	1.5170	1.6949	1.5156

high birefringence (Δn ~ 0.20–0.28) liquid crystals have n_o ~ 1.50–1.52. These are the mixtures of cyano-biphenyls and cyano-terphenyls, *e.g.,* Merck E-series and BL-series. Only some high birefringence (Δn = 0.4) LCs have n_o > 1.55. These are mainly isothiocyanato-tolane mixtures, *e.g.,* UCF-series. Thus, we compare the index matching of some Merck E-series (E7, E48, and E44) and BL-series (BL003, BL006, and BL038) liquid crystals with NOA65, and some high birefringence UCF mixtures (UCF-1 and UCF-2) with NOA81.

Figure 4 shows the measured refractive index of the UV-cured NOA65 and the ordinary refractive index of E48, E44, and E7, as a function of wavelength at T = 20°C. The filled circles, open squares, upward triangles, and downward triangles are the measured ordinary refractive index of NOA65, E48, E44, and E7, respectively. The respective solid lines represent the fittings of each material using the extended Cauchy model [Eq. (2)]. The fitting parameters A, B, and C are listed in Table 4. From Fig. 4, E48, E44, and E7 all have a reasonably good index matching with NOA65. The mismatch is within 0.005 at λ = 550 nm. More specifically, E44 has the best match in the red spectral region while E7 and E48 have the best match in the blue region. In the green region (λ = 546 nm), E44 has a slightly higher index, while E7 and E48 are slightly lower than NOA65, but the difference is in the third decimal.

Figure 5 shows the refractive index of the cured NOA65 and the ordinary refractive index of BL038, BL006,

TABLE 6 — The measured refractive indices (n_e and n_o) of E44 at λ = 450, 486, 546, 589, 633, and 656 nm at different temperatures.

T	λ (nm) 450		486		546		589		633		656	
(°C)	n_e	n_o	n_e	n_o	n_e	n_o	n_e	n_o	n_e	n_o	n_e	n_o
15	1.8652	1.5509	1.8393	1.5429	1.8102	1.5338	1.7960	1.5295	1.7856	1.5259	1.7807	1.5245
20	1.8607	1.5485	1.8339	1.5415	1.8048	1.5330	1.7906	1.5285	1.7806	1.5245	1.7760	1.5233
25	1.8539	1.5478	1.8279	1.5408	1.7993	1.5322	1.7855	1.5275	1.7754	1.5242	1.7709	1.5221
30	1.848	1.5491	1.8221	1.5407	1.7934	1.5315	1.7800	1.5269	1.7699	1.5233	1.7653	1.5222
35	1.8408	1.5464	1.8155	1.5393	1.7874	1.5308	1.7742	1.5262	1.7643	1.5226	1.7595	1.5213
40	1.8338	1.5474	1.8089	1.5391	1.7809	1.5296	1.7679	1.5251	1.7579	1.5217	1.7533	1.5198
45	1.8262	1.5464	1.8018	1.5389	1.7747	1.5298	1.7614	1.5250	1.7516	1.5208	1.7473	1.5196
50	1.8192	1.5468	1.7948	1.5384	1.7679	1.5291	1.7547	1.5246	1.7454	1.5211	1.7410	1.5198
55	1.8111	1.5464	1.7871	1.5384	1.7604	1.5289	1.7480	1.5244	1.7384	1.5202	1.7343	1.5189

TABLE 7 — The measured refractive indices (n_e and n_o) of E7 at λ = 450, 486, 546, 589, 633, and 656 nm at different temperature.

T	λ (nm) 450		486		546		589		633		656	
(°C)	n_e	n_o	n_e	n_o	n_e	n_o	n_e	n_o	n_e	n_o	n_e	n_o
15	1.817	1.5435	1.7921	1.536	1.7664	1.5273	1.7542	1.523	1.7446	1.5197	1.7407	1.5179
20	1.8084	1.5431	1.7847	1.5357	1.7589	1.5269	1.7466	1.5227	1.7378	1.5188	1.7338	1.5177
25	1.8005	1.5424	1.7763	1.5353	1.7512	1.5268	1.7394	1.5225	1.7305	1.5189	1.7263	1.5176
30	1.7909	1.543	1.7679	1.5357	1.7433	1.5271	1.7317	1.5226	1.7229	1.5189	1.719	1.5177
35	1.7811	1.5448	1.7581	1.5369	1.7344	1.5277	1.7231	1.5231	1.7142	1.5191	1.7102	1.5179
40	1.7695	1.547	1.7472	1.5383	1.7237	1.5287	1.7124	1.5239	1.7037	1.5205	1.7001	1.5189
45	1.7549	1.5491	1.7333	1.5406	1.7109	1.5308	1.7001	1.5261	1.6919	1.5221	1.6882	1.5206
50	1.7355	1.5538	1.7154	1.5449	1.6941	1.535	1.6837	1.5299	1.6761	1.526	1.6721	1.5246
55	1.6936	1.569	1.6779	1.5588	1.6601	1.5479	1.6511	1.5428	1.644	1.5377	1.6405	1.5353

and BL003 as a function of wavelength at T = 20°C. The filled circles, open squares, upward triangles, and downward triangles are the measured ordinary refractive index of NOA65, BL038, BL006, and BL003, respectively. The solid lines represent the fittings of each material using the extended Cauchy model [Eq. (2)]. The fitting parameters are listed in Table 4. In Fig. 5, BL038, BL006, and BL003 have a similar trend in $n_o(\lambda)$. The index matching with NOA65 is pretty good in the green and red spectral regions. A larger deviation is observed in the blue region, but the difference is still in the third decimal.

The ordinary refractive index of NOA81 is larger than NOA65. The measured value of NOA81 at λ = 589 nm and T = 20°C is 1.5662. No commercially available LC mixtures have such a high n_o. We have formulated two new LC mixtures designated as UCF-1 and UCF-2 whose ordinary refractive index matches with NOA81. Figure 6 shows the refractive index of the cured NOA81 and the ordinary refractive index of UCF-1 and UCF-2 as a function of wavelength at T = 20°C. The filled circles, open squares, and upward triangles

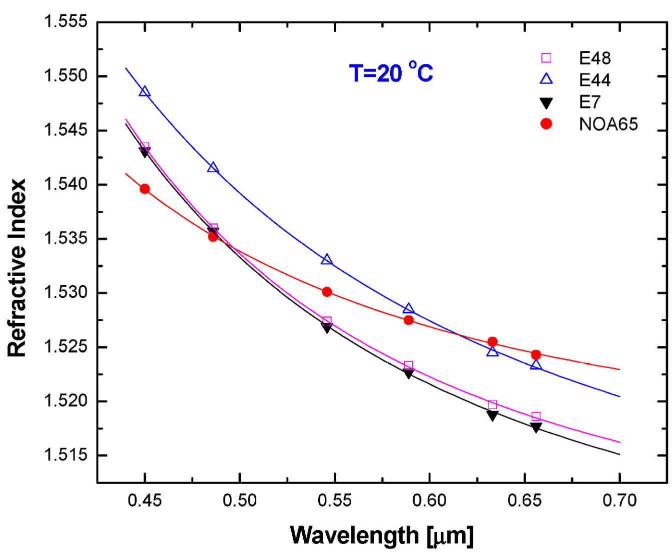

FIGURE 4 — Wavelength-dependent refractive index of NOA65 and the ordinary refractive index of E48, E44 and E7 at T = 20°C. The open squares, upward triangles, filled circles, and downward triangles are the measured refractive index of E48, E44, NOA65 and E7, respectively. The solid lines represent the fittings using the extended Cauchy model [Eq. (2)]. The fitting parameters are listed in Table 4.

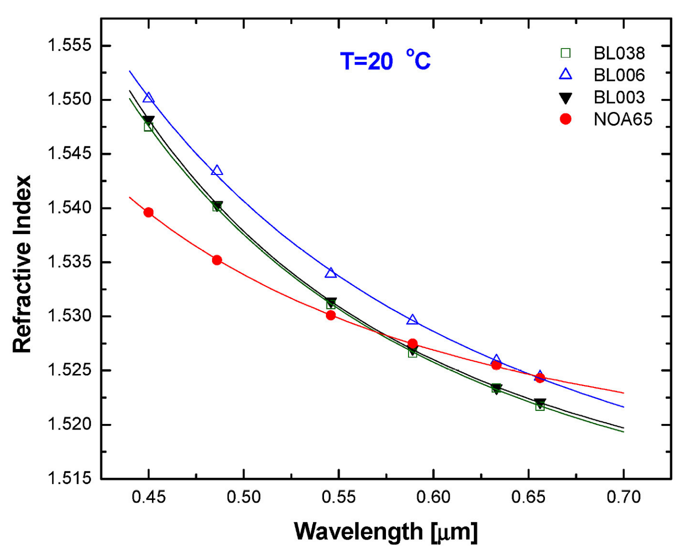

FIGURE 5 — Wavelength-dependent refractive index of NOA65 and the ordinary refractive index of BL038, BL006, and BL003 at T = 20°C. The open squares, upward triangles, filled circles, and downward triangles are the measured refractive index of BL038, BL006, NOA65 and BL003, respectively. The solid lines represent the fittings using the extended Cauchy model [Eq. (2)]. The fitting parameters are listed in Table 4.

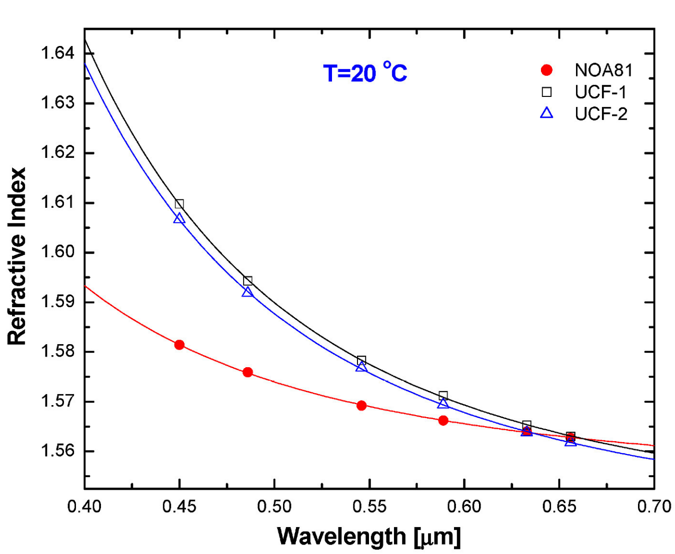

FIGURE 6 — Wavelength-dependent refractive index of NOA81 and the ordinary refractive index of UCF-1 and UCF-2 at T = 20°C. The filled circles, open squares, and upward triangles are the measured refractive index of NOA81, UCF-1, and UCF-2, respectively. The solid lines represent the fittings using the extended Cauchy model [Eq. (2)]. The fitting parameters are listed in Table 11.

are the measured ordinary refractive index of NOA81, UCF-1, and UCF-2, respectively. The solid lines represent the fittings of each material using the extended Cauchy model [Eq. (2)]. The fitting parameters are listed in Table 4. In Fig. 6, the n_o of UCF-1 and UCF-2 match well with that of NOA81 in the red region. As the wavelength gets shorter, the deviation increases gradually. This is because the longest electronic absorption band of the high birefringence LCs usually extends to λ_2 ~ 350-nm region.[17] In the blue spectral region, the resonance effect to the refractive index is more pronounced because the wavelength is closer to λ_2.

In a PDLC system, good index matching ($n_o \sim n_p$) between the employed polymer and liquid crystal helps to improve the transmittance in the voltage-on state. On the other hand, a larger index mismatch ($\langle n \rangle > n_p$), *i.e.*, a higher birefringence LC enhances the light-scattering efficiency in the voltage-off state. However, refractive-index match or mismatch is not the only factor deciding the PDLC performance. UV stability of liquid crystals and miscibility between polymers and liquid crystals also play important roles affecting the PDLC properties. As we discussed before, the E-series and BL-series liquid crystals all have a good index match with NOA65. All these six liquid crystals are good candidates for PDLC application when NOA65 is used. In the visible spectrum, E48 and E7 have very similar ordinary refractive index at T = 20°C, as do BL038 and BL003. However, E48 (BL038) has a higher birefringence than E7 (BL003). Thus, we choose to compare the NOA65 PDLC systems using BL038, E48, BL006, and E44.

4 PDLC cell fabrication and measurements

To prepare PDLC samples, we mixed NOA65 with E48, E44, BL038, and BL006; each at a 30:70 wt.% ratio. To ensure a uniform mixing, we stirred the LC/monomer mixtures using small magnetic stirrers for half an hour at T = 120°C. Each LC/monomer mixture was then injected to an empty glass cell (cell gap ~8 μm) in the isotropic state. The inner surfaces of the glass substrates were coated with a thin indium-tin-oxide layer, but no polyimide layer. To cure the samples, the cells were exposed to UV light (I = 65 mW/cm^2, λ ~ 365 nm) for 15 minutes at T = 20°C.

The voltage-dependent transmittance (VT) curves were measured and used to compare the contrast ratio of the PDLC cells. The experimental setup is shown in Fig. 7.

TABLE 8 — The measured refractive indices (n_e and n_o) of BL038 at λ = 450, 486, 546, 589, 633, and 656 nm at different temperature.

T	λ (nm)											
	450		486		546		589		633		656	
(°C)	n_e	n_o	n_e	n_o	n_e	n_o	n_e	n_o	n_e	n_o	n_e	n_o
15	1.8796	1.5478	1.8511	1.5407	1.8196	1.5323	1.8047	1.5276	1.794	1.5239	1.7887	1.5228
20	1.8726	1.5475	1.8450	1.5401	1.8142	1.5311	1.7994	1.5266	1.7888	1.5234	1.7833	1.5217
25	1.8671	1.5469	1.8392	1.5396	1.8086	1.5305	1.7939	1.5258	1.7832	1.5221	1.7786	1.5209
30	1.8611	1.5458	1.8334	1.5385	1.8029	1.5299	1.7884	1.5250	1.7781	1.5213	1.7729	1.5199
35	1.8544	1.5457	1.8271	1.538	1.7971	1.5291	1.7827	1.5241	1.7721	1.5206	1.7675	1.5190
40	1.8481	1.5447	1.8206	1.5375	1.7907	1.5284	1.7767	1.5239	1.7662	1.5200	1.7618	1.5181
45	1.8401	1.5446	1.8137	1.537	1.7846	1.5277	1.7704	1.5231	1.7603	1.5194	1.7554	1.5179
50	1.8325	1.5444	1.8066	1.5369	1.7778	1.5272	1.7641	1.5227	1.7541	1.5187	1.7491	1.5169
55	1.8252	1.5441	1.7992	1.5363	1.7709	1.5269	1.7571	1.5222	1.7475	1.5183	1.7430	1.5170

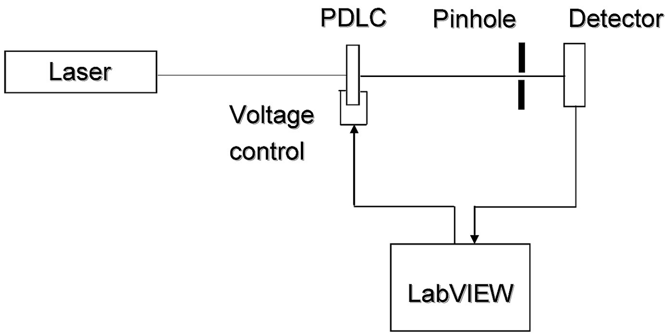

FIGURE 7 — The experimental setup for measuring the transmittance of the PDLC cells.

An unpolarized He-Ne laser (λ = 633 nm) beam was normally incident on the PDLC cell. A photodiode detector was placed at 25 cm behind the cell. The corresponding collection angle is ~2°. A LabVIEW data acquisition system was used to control the applied voltage and record the measured VT curves.

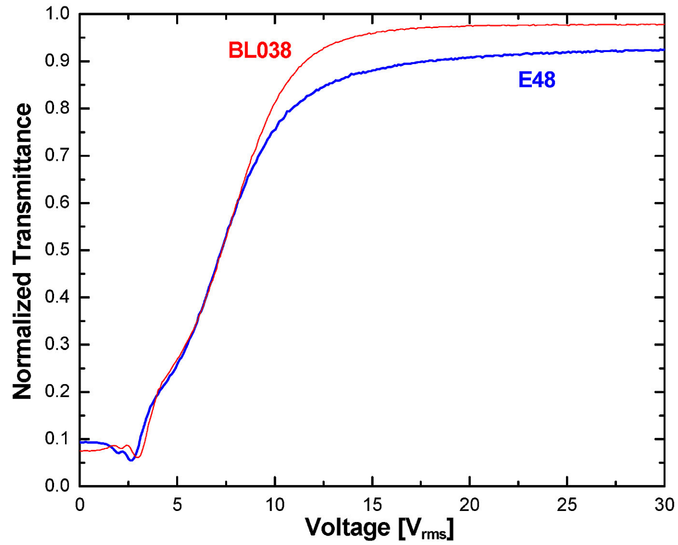

FIGURE 8 — Voltage-dependent normalized transmittance of the BL038 and E48 PDLC cells at λ = 633 nm. For both cells, the LC:NOA65 ratio is 70:30. The two cells have same thickness (d = 8 μm) and have no polyimide layer on the glass substrates.

5 Results and discussion

From the measured VT curves, we find that BL038 is better than BL006, and E48 is better than E44 in the NOA65 PDLC systems, although these four LC mixtures all have a good index match with NOA65. The BL038 PDLC and E48 PDLC cells exhibit a lower transmittance in the voltage-off state and a higher transmittance in the voltage-on state than that of BL006 PDLC and E44 PCLC cells, respectively. It implies that the refractive index match is not the only factor affecting the contrast ratio of a PDLC; the LC/polymer miscibility also plays an important role. It is likely that BL038 and E48 have a better miscibility in NOA65 than BL006 and E44.

In Fig. 8, we compare the normalized VT curves of the BL038 and E48 PDLC cells at λ = 633 nm. For both cells, the polymer (NOA65) and LC ratio is 30:70 and cell gap is 8 μm. To calibrate the substrate reflection losses, the transmittance of the PDLC cell is normalized to that of a homogeneous cell filled with the corresponding liquid crystal. The red line represents the transmittance of the BL038 PDLC cell and the blue line represents the transmittance of the E48 PDLC cell. In Fig. 8, the BL038 PDLC cell has a lower transmittance at V = 0 and a higher transmittance in

TABLE 9 — The measured refractive indices (n_e and n_o) of BL006 at λ = 450, 486, 546, 589, 633, and 656 nm at different temperature.

T (°C)	450 n_e	450 n_o	486 n_e	486 n_o	546 n_e	546 n_o	589 n_e	589 n_o	633 n_e	633 n_o	656 n_e	656 n_o
15	1.8988	1.5478	1.8672	1.5438	1.8349	1.5348	1.8194	1.5304	1.8083	1.5266	1.8033	1.5257
20	1.8913	1.5516	1.8620	1.5434	1.8299	1.5339	1.8148	1.5296	1.8036	1.5259	1.7986	1.5244
25	1.8869	1.5505	1.8563	1.5421	1.8248	1.5331	1.8097	1.5285	1.7988	1.5249	1.7937	1.5236
30	1.8811	1.5479	1.8508	1.5414	1.8194	1.5323	1.8046	1.5275	1.7937	1.5239	1.7884	1.5224
35	1.8760	1.5482	1.8449	1.5405	1.8140	1.5312	1.7994	1.5266	1.7885	1.5229	1.7835	1.5215
40	1.8702	1.5472	1.8391	1.5399	1.8084	1.5306	1.7938	1.5257	1.7830	1.5221	1.7784	1.5206
45	1.8630	1.5454	1.8328	1.5387	1.8024	1.5294	1.7880	1.5249	1.7774	1.5211	1.7726	1.5200
50	1.8566	1.5447	1.8265	1.5382	1.7964	1.5292	1.7822	1.5245	1.7721	1.5204	1.7672	1.5192
55	1.8486	1.5441	1.8200	1.5377	1.7905	1.5286	1.7764	1.5238	1.7659	1.5199	1.7613	1.5181

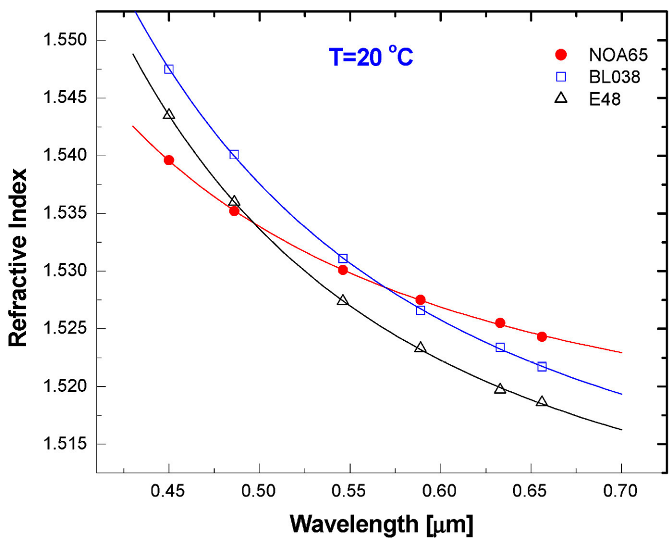

FIGURE 9 — Wavelength-dependent refractive index of NOA65 (circles) and the ordinary refractive index of BL038 (squares) and E48 (triangles) at T = 20°C. The solid lines represent the fittings using the extended Cauchy model [Eq. (2)]. The fitting parameters are listed in Table 4.

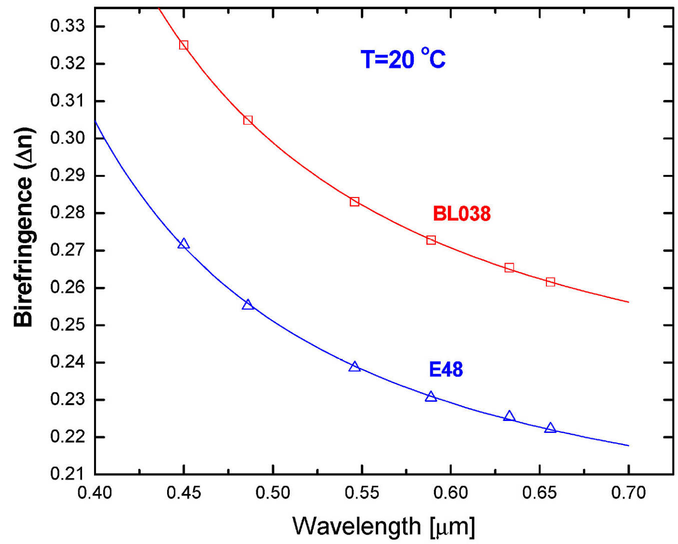

FIGURE 10 — Wavelength-dependent birefringence of BL038 (squares) and E48 (triangles) at T = 20°C. The solid lines are fittings using the single-band model [Eq. (3)]. The fitting parameters [G(μm^{-2}), λ*(μm)] for BL038 and E48 are [3.509, 0.252] and [3.210, 0.244], respectively.

the on-state than E48. The saturation voltage of both cells happens at ~20 V_{rms}, thus, we define the contrast ratio as: $CR = T(V = 20\ V_{rms})/T(V = 0)$. The measured contrast ratio is 13:1 and 10:1 for the BL038 and E48 PDLC cells, respectively. We could enhance contrast ratio by using a thicker cell gap. The tradeoff is the increased operating voltage.

Two factors contributing to the higher contrast ratio of the BL038 PDLC cell over E48 are higher birefringence and better index matching with NOA65. In Fig. 9, we compare the wavelength-dependent refractive index of NOA65 and the ordinary refractive index of BL038 and E48 at T = 20°C. The filled circles, open squares, and upward triangles are the measured refractive index of NOA65, BL038, and E48, respectively. The solid lines represent the fittings using the extended Cauchy model [Eq. (2)]. The fitting parameters are listed in Table 4. From Fig. 9, we find that BL038 has a better index match than E48 at λ = 633 nm. Thus, the BL038 PDLC cell has a higher transmittance in the voltage-on state than the E48 cell when the He–Ne laser (λ = 633 nm) is used. However, this explanation is only qualitative. In the voltage-on state, the LC directors near the inner boundaries of the droplets are harder to be reoriented by the electric field because of the surface anchoring effect. These anchored LC directors have some n_e components. As a result, the effective refractive index in the voltage-on state

TABLE 10 — The measured refractive indices (n_e and n_o) of BL003 at λ = 450, 486, 546, 589, 633, and 656 nm at different temperature.

	λ (nm)											
T	450		486		546		589		633		656	
(°C)	n_e	n_o	n_e	n_o	n_e	n_o	n_e	n_o	n_e	n_o	n_e	n_o
15	1.8654	1.5489	1.8374	1.5408	1.8082	1.5324	1.7943	1.5279	1.7838	1.5246	1.7793	1.5235
20	1.8592	1.5472	1.8316	1.5403	1.8030	1.5314	1.7891	1.5270	1.7790	1.5234	1.7742	1.5221
25	1.8541	1.5477	1.8260	1.5390	1.7973	1.5306	1.7837	1.5260	1.7736	1.5224	1.7691	1.5216
30	1.8473	1.5451	1.8199	1.5388	1.7916	1.5302	1.7780	1.5254	1.7682	1.5215	1.7636	1.5204
35	1.8415	1.5443	1.8135	1.5379	1.7857	1.5293	1.7723	1.5246	1.7625	1.5210	1.7577	1.5192
40	1.8334	1.5444	1.8071	1.5375	1.7794	1.5284	1.7661	1.5238	1.7564	1.5203	1.7521	1.5190
45	1.8255	1.5447	1.8001	1.5369	1.7728	1.5279	1.7598	1.5234	1.7501	1.5197	1.7458	1.5186
50	1.8186	1.5444	1.7931	1.5366	1.7662	1.5275	1.7534	1.5228	1.7438	1.5193	1.7397	1.5179
55	1.8113	1.5439	1.7855	1.5368	1.7591	1.5276	1.7465	1.5229	1.7367	1.5190	1.7327	1.5176

is slightly larger than n_o It is difficult to estimate how much these boundary layers contribute to the effective refractive index. It should be mentioned that the results shown in Fig. 9 are for convenient demonstration only because of the availability of a He–Ne laser light source. For practical PDLC display, human eyes are more sensitive to green than red. Therefore, the device should be optimized at a green wavelength ($\lambda \sim 550$ nm).

Figure 10 shows the wavelength-dependent birefringence of BL038 and E48 at $T = 20°C$. The squares and triangles represent the experimental data of BL038 and E48, respectively. The solid lines are fittings using the following single-band birefringence dispersion model[18]:

$$\Delta n(\lambda) = G\frac{\lambda^2\lambda^{*2}}{\lambda^2 - \lambda^{*2}}, \quad (3)$$

where G is a proportionality constant and λ^* is the mean resonant wavelength of the liquid crystal. The fitting parameters [G (μm^{-2}), λ^* (μm)] for BL038 and E48 are [3.509, 0.252] and [3.210, 0.244], respectively. In Fig. 10, BL038 exhibits a larger birefringence than E48 in the entire visible spectral region. Thus, the difference between the average refractive index of BL038 and the refractive index of NOA65 is larger than that between E48 and NOA65, *i.e.*, the refractive-index mismatch between BL038 and NOA65 is larger than that between E48 and NOA65. A larger index mismatch leads to a higher scattering efficiency. As a result, the BL038 PDLC cell has a lower transmittance at $V = 0$ than the E48 cell.

6 Conclusion

The refractive index of cured polymers, NOA65 and NOA81, were measured at six visible wavelengths and in the temperature range from 20 to 55°C using a multi-wavelength Abbe refractometer. The refractive indices of Merck E-series (E48, E44, and E7) and BL-series (BL038, BL006, and BL003) LC mixtures were measured. Comparative study on the refractive index between these liquid crystals and cured polymers was made. Among the LC materials we studied, BL038 and E48 are good candidates for making PDLC system incorporating NOA65. Indeed, the BL038 PDLC cell shows a higher contrast ratio than the E48 cell because BL038 has a better-matched ordinary refractive index, higher birefringence, and similar miscibility as compared to E48. Liquid crystals having a good miscibility with polymer, matched ordinary refractive index, and higher birefringence help to improve the PDLC contrast ratio for display applications.

References

1 J L Fergason, "Polymer encapsulated nematic liquid crystals for display and light control applications," *SID Symposium Digest Tech Papers* **16**, 68–69 (1985).

2 J W Doane, A Golemme, B G Wu, and S Zumer, "Field controlled light scattering from nematic microdroplets," *Appl Phys Lett* **48**, 269–271 (1986).

3 P S Drzaic, *Liquid Crystal Dispersions* (World Scientific, Singapore, 1995).

4 S T Wu and D K Yang, *Reflective Liquid Crystal Displays* (New York, Wiley, 2001).

5 S Matsumoto, M Houlbert, T Hayashi, and K Kubodera, "Fine droplets of liquid crystals in a transparent polymer and their response to an electric field," *Appl Phys Lett* **69**, 1044–1046 (1996).

6 S Matsumoto, K Hirabayashi, S Sakata, and T Hayashi, "Tunable wavelength filter using nano-sized droplets of liquid crystal," *IEEE Photonics Technol Lett* **11**, 442–444 (1999).

7 D E Lucchetta, R Karapinar, A Manni, and F Simoni, "Phase-only modulation by nanosized polymer-dispersed liquid crystals," *J Appl Phys* **91**, 6060–6065 (2002).

8 H Ren, Y H Fan and S T Wu, "Tunable Fresnel lens using nanoscale polymer-dispersed liquid crystals," *Appl Phys Lett* **83**, 1515–1517 (2003).

9 H Ren, Y H Fan, Y H Lin, and S T Wu, "Tunable-focus microlens arrays using nanosized polymer-dispersed liquid crystal droplets," *Opt Commun* **247**, 101–106 (2005).

10 H Ren, Y H Lin, Y H Fan, and S T Wu, "Polarization-independent phase modulation using a polymer-dispersed liquid crystal," *Appl Phys Lett* **86**, 141110 (2005).

11 Y H Fan, Y H Lin, H Ren, S Gauza, and S T Wu, "Fast-response time and scattering-free polymer network liquid crystals for infrared light modulators," *Appl Phys Lett* **84**, 1233–1235 (2004).

12 J Li, S Gauza, and S T Wu, "High temperature-gradient refractive index liquid crystals," *Opt Express* **12**, 2002–2010 (2004).

13 J Li, S Gauza, and S T Wu, "Temperature effect on liquid crystal refractive indices," *J Appl Phys* **96**, 19–24 (2004).

14 S T Wu, C S Wu, M Warenghem, and M Ismaili, "Refractive-index dispersions of liquid-crystals," *Opt Eng* **32**, 1775–1780 (1993).

15 J Li and S T Wu, "Extended Cauchy equations for the refractive indices of liquid crystals," *J Appl Phys* **95**, 896–901 (2004).

16 J Li and S T Wu, "Two-coefficient Cauchy model for low birefringence liquid crystals," *J Appl Phys* **96**, 170–174 (2004).

17 S Gauza, C H Wen, N Janarthanan, C S Hsu, and S T Wu, "Super high birefringence isothiocyanato biphenyl-bistolane liquid crystals," *Jpn J Appl Phys* **43**, 7634–7638 (2004).

18 S T Wu, "Birefringence dispersions of liquid crystals," *Phys Rev A* **33**, 1270–1274 (1986).

Jun Li is a Ph.D. candidate at the College of Optics and Photonics, University of Central Florida, Orlando, Florida. He received his B.S. degree in mechanical engineering and M.S. degree in automation, both from Tsinghua University, P. R. China. His current research is to develop structure-property correlation of liquid crystals, novel liquid-crystal materials with high dn_o/dT at room temperature for highly thermal tunable liquid-crystal photonic crystal bandgap fibers, and measurements of liquid-crystal refractive indices in the visible and infrared spectral regions. His future work will focus on the polymer-dispersed liquid crystal, microdisplay technology, and novel liquid crystals for display and photonic applications.

Greg Baird is a junior at the University of Missouri-Rolla majoring in ceramic engineering. He has worked the past four years for a specialty glass manufacturing company Mo-Sci. He has been involved in many projects that include: crown cementation glass, NVIS glass, and glass microspheres among others. Outside of the classroom Greg has been involved in multiple competing engineering teams. He was part of a design team that took first place in the 2004 American Ceramic Society's annual ceramic putter competition, and also a team that received an honorable mention in the National Hydrogen Association's 2004 hydrogen design contest. In 2005, Greg joined UCF for the summer through the NSF-sponsored research experience for undergraduates program.

Yi-Hsin Lin is a Ph.D. candidate at the College of Optics and Photonics, University of Central Florida, Orlando, Florida. She received her M.S. degree in electro-optical engineering from National Chiao Tung University, and B.S. in physics from National Tsinghua University, Taiwan. Her current research is to develop novel polarization-independent liquid-crystal devices, novel liquid-crystal displays, and fast-response infrared phase modulators for optical communications.

Hongwen Ren received his Ph.D. from Changchun Institute of Optics, Chinese Academy of Sciences, China. He joined the College of Optics and Photonics, University of Central Florida as a research scientist in 2001. He is currently engaged in the research of liquid-crystal photonics for optical communications, electrically tunable liquid-crystal lens and liquid lens for zoom lens applications, and polymer-stabilized liquid crystals for fast-response polarization independent phase modulators.

Shin-Tson Wu is a PREP Professor at the College of Optics and Photonics, University of Central Florida. Prior to joining UCF in 2001, Dr. Wu worked at Hughes Research Laboratories (Malibu, California) for 18 years. He received his Ph.D. from the University of Southern California and his B.S. in physics from National Taiwan University. His studies at UCF concentrate in foveated imaging, bio-photonics, optical communications, liquid-crystal displays, and liquid-crystal materials. Dr. Wu is a Fellow of the IEEE, SID, and OSA. He has co-authored two books: *Reflective Liquid Crystal Displays* (Wiley, 2001) and *Optics and Nonlinear Optics of Liquid Crystals* (World Scientific, 1993).